5896 *Macromolecules* **2010**, *43*, 5896–5903
DOI: 10.1021/ma100734r

Macromolecules
ARTICLE

Transport of Star-Branched Polymers in Nanoscale Pipe Channels Simulated with Dissipative Particle Dynamics Simulation

Ziqi Li,[†,‡] Yajie Li,[‡] Yongmei Wang,*[,‡] Zhaoyan Sun,*[,†] and Lijia An[†]

[†]*State Key Laboratory of Polymer Physics and Chemistry, Changchun Institute of Applied Chemistry, Chinese Academy of Sciences, Changchun, 130022, P. R. China, and* [‡]*Department of Chemistry, The University of Memphis, Memphis, Tennessee 35154*

Received April 5, 2010; Revised Manuscript Received May 26, 2010

ABSTRACT: Transport of star polymers under pressure-driven flow in a pipe with pipe radius being at least twice the size of polymers has been examined with standard dissipative particle dynamics (DPD) simulations. Equilibrium dynamics of star polymers in bulk solution were found to obey the Zimm model very well, indicating that DPD simulation correctly incorporates the hydrodynamic interaction in the stars. Under pressure-driven flow, star polymers with more arms were found to migrate toward the center of pipe more, leading to a net faster velocity and hence a shorter retention time in the pipe. The stretching of star polymers along the flow was found to follow similar scaling behavior as the linear polymer chains, except that the Weissenberg number Wi for the stars should be reduced by arm number f. After rescaling of the Weissenberg number, the stretch ratio S_x, defined as the ratio of square of radius gyration of the chains along the flow, ${R_{gx}}^2$, over its corresponding value in dilute bulk solution, was found to scale with Wi linearly when $Wi \gg 1$. The compression of the chains in the dimension perpendicular to the flow S_y were found to scale with $Wi^{-0.5}$ when $Wi \gg 1.0$.

1. Introduction

Elucidating the equilibrium conformation, dynamic, and transport properties of star branched polymers has been an important subject in polymer physics very early on.[1−12] Theoretical works like the early work by Zimm and Stockmayer[1] and scaling theory proposed by Daoud and Cotton[2] have become the reference point of discussions on properties of star polymers. Several recent books in polymer physics[13,14] have also provided good summaries about known equilibrium and dynamic properties predicted by these theories and to some extent confirmed by experiments. Computer simulations of star polymers have also been numerous[4,6−12,15−19] since simulations can provide missing microscopic link between theories and experimental observation. While equilibrium properties of star polymers could been examined by Monte Carlo or molecular dynamics simulations,[4,8−10,12] capturing dynamic and transport properties of star polymers in dilute solution correctly in computer simulations was not possible[20] until in recent years when a number of mesoscopic simulation techniques that can account for hydrodynamic interaction in solution have been developed.[21−29]An important requisite of such simulation methods is the momentum conservation. The original Brownian dynamic simulations do not account for hydrodynamic interaction correctly,[20] although an approximate method using Oseen tensor now becomes an acceptable approach. Other simulation methods that can account for hydrodynamic interaction, reviewed recently by Slater et al.,[30] include the lattice−Boltzmann method,[27−29] multiparticle-collision dynamics (MPC),[24−26] and dissipative particle dynamics (DPD).[21−23] These methods, though generally are accepted as capable of accounting for hydrodynamic interaction, are not without problems. For example, DPD has been criticized for having low Schmidt number, and hence its capability to model real polymers like polystyrene in solvents like water or toluene is questionable. Alternative modified DPD methods that yield higher Schmidt number[31,32] have been proposed and have been used to simulate polymer dynamics under flow. Several studies have shown that the observed chain stretching and the migration pattern of the chain in the channel are affected by simulation methods with different Schmidt number.[33,34] Earlier, we have carefully examined polymer dynamics simulated with standard DPD[35] and found that the dynamics of linear polymer chain follow the known Zimm model well, which indicates that the hydrodynamic interaction between polymer beads mediated by solvents is reasonably captured in DPD simulation. Therefore, the claimed critics against DPD having low Schmidt number and hence unable to capture the hydrodynamic interaction between polymer beads may not be true.

Although molecular dynamic simulations of star polymers were performed extensively by Grest et al.,[4,8] star polymers simulated in their studies were not immersed in a solvent bath. Dynamics revealed in these simulations obey the Rouse model as opposed to the Zimm model. Simulations of transport of star branched polymers in solution have not been extensively investigated so far. Ripoll et al.[36,37] used MPC to examine dynamics of star polymers in simple shear flow. In their first paper, they focused on conformational change of star polymers during the shear flow. They found star polymers exhibit a crossover in their properties from those of linear polymers to a novel behavior which resembles the tank-treading motion of elastic capsules at high number of arms. In their second paper, they characterized the flow field near the star polymers and found that flow fields are strongly perturbed around the stars. The more the number of arms, the stronger the perturbation on the fluid velocity.[36] More recently, Nardai and Zifferer[38] reported a DPD simulation of dilute solutions of star-branched polymers. They focused on analysis of equilibrium dynamics of star polymers as revealed

*Corresponding authors. E-mail: ywang@memphis.edu (Y.W.); zysun@ciac.jl.cn (Z.S.).

 Published on Web 06/08/2010

in DPD simulations at both athermal and theta solvent. The Zimm behavior of star polymers is again observed in their DPD simulations.

We are interested in the transport of star polymers in nanoscale channels from two perspectives. First, similar to Ripoll et al., we would like to understand the interplay between conformational change of star polymers under flow, but not in shear flow, instead in Poiseuille-like flow. Such investigations are relevant to the understanding of a number of processes like blood circulation in the human body. Second, we are interested from the perspective of separation of star polymers from linear polymers in hydrodynamic chromatography (HDC). HDC is a terminology used in separation science which refers to a simple process where solutes, typically colloids or macromolecules, are transported through a conduit with a Poiseuille-like flow. HDC is related to the family of field-flow-fractionation (FFF) methods. The development of microfluidic devices has led to development of on-chip hydrodynamic chromatography[39−42] where a single long micrometer sized channel is used as the separation medium. A basic question here is whether star polymers, when transported through the channel under pressure-driven flow, will move faster or slower than the linear polymers with equivalent size. This question has not and could not been easily answered with the current status of knowledge.

Earlier we reported DPD simulations of HDC separation of linear polymers in a slit channel.[43] Simulation reveals that chain stretch can significantly distort retention behavior of linear polymers and lead to reversal in elution order. In the current study, we focus on the transport of star-branched polymer in cylindrical pipe under pressure-driven flow, and we compare the behavior between star-branched polymers against linear polymer chains.

2. Simulation Method

We used the standard dissipative particle dynamics as implemented in several of our earlier studies.[35,43,44] Details of the simulations follow closely to that reported in our most recent paper.[43] Briefly, solvent particles are coarse-grained into fluid elements, called DPD particles, which interact with each other through three pairwise interaction forces:

$$f_{i,j} = F_{ij}^{(C)} + F_{ij}^{(D)} + F_{ij}^{(R)}$$

where $F_{ij}^{(C)}$ is the conservative force, $F_{ij}^{(D)}$ is the dissipative force, and $F_{ij}^{(R)}$ is the random force acting on the ith particle from jth particles. The forms of these interactions follow the standard functions as used by Groot and Warren.[21] We have chosen the mass of the DPD particles m, the cutoff distance r_c used in the pairwise interactions, and the thermal energy k_BT as the fundamental units in all reported quantities. The motions of particles are numerically solved with the modified velocity-Verlet algorithm. All our simulations are performed for DPD fluids with a particle number density $\rho = 3.0{r_c}^{-3}$, $k_BT = 1$, conservative force $a_{ij} = 25k_BT/r_c$, and friction coefficient $\sigma = 3((k_BT)^3m/{r_c}^2)^{1/4}$.

The polymer chain is modeled by connecting fluid DPD particles via an additional finite extensible potential between consecutive beads belong to the same chain:

$$U_{\text{intra}}(r_{i,i+1}) = \begin{cases} \dfrac{-K_F}{2}(r_{\max}-r_{eq})^2 \ln\left[1-\left(\dfrac{r_{i,i+1}-r_{eq}}{r_{\max}-r_{eq}}\right)^2\right] & (\text{for } r_{i,i+1} < r_{\max}) \\ \infty & (\text{for } r_{i,i+1} \geq r_{\max}) \end{cases} \quad (1)$$

We have set $r_{\max} = 2.0r_c$, $r_{eq} = 0.7r_c$, and $K_F = 40k_BT/r_c$. Both static and equilibrium dynamic properties of linear polymer chains modeled with the above DPD model have been thoroughly characterized in our earlier study.[35] In the current study, we extend this model to star-branched polymers. The star polymers are composed of f arms with equal length, connected to a center DPD particle. The total number of DPD particles in a star $N_{tot} = fN_a + 1$, where N_a is the number of DPD particles on each arm. In all reported simulations, N_a was varied from 5, 10, 15, 20 to as high as 60, while the number of arms f was varied from 2 (linear), 3, 4, 5 to as high as 10.

The fluid channel modeled in the current study is a cylindrical pipe with a length of $L = 60r_c$. The pipe radius R_p varied from $5r_c$ to $10r_c$. The total number of DPD particles in simulation is typically around ∼10 000 to ∼55 000 depending on the pipe radius. The pipe boundary was modeled by a combination of using solid static wall particles and a simple bounce back condition. Four layers of static DPD particles, packed in hexagonal lattice of unit length $0.25r_c$, were built at the outer surface of the pipe. These static DPD wall particles interact in the usual manner with fluid DPD particles, except the repulsive part of interaction force $a = 3k_BT/r_c$. However, the presence of solid walls cannot fully prevent DPD fluid particles getting out of the pipe. Therefore, we applied an additional simple bounce-back condition to all fluid DPD particles, including both solvent and polymer particles. In simple bounce back, if the particle will go out of the boundary during the integration step, the particle is put back to its original position with a reversed velocity. This boundary condition is enforced at every step. The pressure driven flow is achieved by applying a body force f_x in x direction to all DPD particles. The force f_x is varied from 0.0 to $0.05k_BT/r_c$. The average velocity $\langle u \rangle$ in Poiseuille flow within a pipe is given by

$$\langle u \rangle = \frac{1}{2}u_{\max} = \frac{1}{8\eta}\frac{\Delta P}{L}{R_p}^2 \quad (2)$$

where the η is viscosity and ΔP is the pressure drop in pipe which is related to f_x through $\rho f_x = \Delta P/L$. As the pipe length L was kept constant, the average velocity $< u >$ is only dependent on R_p and f_x. The volume fraction of star polymers is kept below 0.02. Equilibrium dynamics properties of star branched polymers were examined with the same DPD model but in a cubic box of $30r_c$x$30r_c$x$30r_c$ with periodic boundary conditions applied in all three directions.

3. Results and Discussion

3.1. Equilibrium Static and Dynamic Properties. We first present our results on equilibrium static and dynamic properties of star polymers. The theoretical studies on the subject can be broadly divided to two main categories: the earlier work by Zimm and Stockmayer,[1] who used Gaussian chain models, and the scaling theory proposed by Daoud and Cotton[2] and later by Birshtein and Zulina.[3] Zimm and Stockmayer defined g factors to quantify the difference of star polymers from that of linear polymers with the same total molecular weight. The static g factor is defined as the ratio of mean-square radius of gyration of stars and linear chains with equal number of segments

$$g(f) = \langle {R_g}^2 \rangle_f / \langle {R_g}^2 \rangle_{f=2} \quad (3)$$

where f is the number of arms in the star. Using Gaussian chain model, Zimm and Stockmayer showed that $g(f) \sim (3f-2)/f^2$ when the chain length $N_{tot} \gg 1$. Because this prediction is based on Gaussian chain model, it is believed to be only applicable in θ solvents. The scaling theory proposed by Daoud and Cotton, on the other hand, attempts to address the excluded volume interaction within the stars. The main

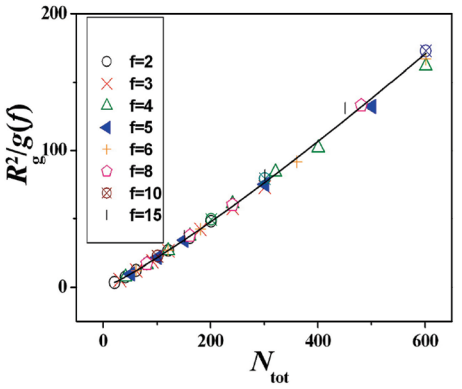

Figure 1. Plot of mean-square radius of gyration of star over $g(f) = ((3f-2)/f^2$ as a function of total polymerization N_{tot} in the stars. Data sets for a given arm number f are stars with arm length N_a varied from $N_a = 10$ to 100. The solid line is the power-law fit with exponent $N_{tot}^{1.18}$.

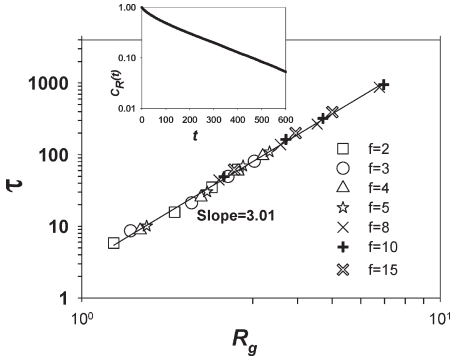

Figure 2. The log−log plot of the relaxation time τ computed from end-to-center autocorrelation, as a function radius of gyration $\langle R_g \rangle$ for stars with number of arms f indicated and arm length N_a varied from 10 to 100. Solid line is the power-law fit with exponent $\tau \sim R_g^{3.0}$. The inset shows an example of decay of the center-to-end vector correlation function, $C_R(t)$, for a star with arm number $f = 4$ and arm length $N_a = 30$.

theoretical results have been summarized by Grest.[8] The scaling theories predict that mean-square radius of gyration $\langle R_g^2 \rangle$ and center-to-end distance $\langle R^2 \rangle$ are given by

$$\langle R^2 \rangle \sim \langle R_g^2 \rangle \propto N_a^{2\nu} f^{1-\nu} = N_{tot}^{2\nu} f^{1-3\nu} \quad (4)$$

We found that the g factor proposed by Zimm and Stockmayer works very well for stars with excluded volume interaction. Several earlier studies have also found this to be true.[9] Figure 1 presents the plot of $\langle R_g^2 \rangle / g(f)$ as a function of N_{tot} for several sets of stars with different number of arms, where $\langle R_g^2 \rangle$ is the radius gyration of the star determined directly in the simulations. Data from different sets form one single master curve with a power dependence on $N_{tot}^{1.18}$, an exponent we got for linear polymers with excluded volume interaction.[35] Small deviations from the master plot can be seen for high number of arms. Taking this $g(f)$ to be applicable here, then we would predict that $\langle R_g^2 \rangle / f^2$ for the stars would depend on f as $\langle R_g^2 \rangle \sim (N_a f)^{2\nu}(3f-2)/f^2$ where ν is the Flory's exponent. Taking $f \gg 1$, this can be simplified as $\langle R_g^2 \rangle \sim N_a^{2\nu} f^{2\nu-1}$. The scaling theory however predicts $N_a^{2\nu} f^{1-\nu}$. With simulation data obtained for f limited below 10, it is difficult to differentiate which dependence is more correct. We note our simulation data would also form a master plot if one plots $\langle R_g^2 \rangle / f^{1-3\nu}$ against N_{tot} by taking $\nu = 0.59$, and the quality of master plot is comparable with that in Figure 1. We believe the scaling theory is applicable only at high number of f, much higher than the range of f examined here. Also, this $g(f)$ works well for stars with no excluded volume interaction such as stars generated with random walks. The corresponding master plot for the stars generated with random walks exhibits $N_{tot}^{1.0}$ dependence. On the other hand, using $\langle R_g^2 \rangle / f^{1-3\nu}$ will no longer produce master plot whether $\nu = 0.59$ or $\nu = 0.50$ are used for the stars generated with random walks.

Equilibrium dynamic properties of dilute polymer solution can be studied by either studying its center of mass of diffusion or the relaxation time. Earlier we found that in DPD simulations the center-of-mass diffusion has a strong dependence on box size because of the presence of hydrodynamic interaction. Therefore, in the current study we did not examine the center-of-mass diffusion but only monitored the relaxation time. The relaxation time for the star was determined based on the decay of autocorrelation function of center-to-end vector, $C_R(t)$:

$$C_R(t) = (\langle R(t)R(0) \rangle - \langle R \rangle^2)/(\langle R^2 \rangle - \langle R \rangle^2) \quad (5)$$

where the **R** is the center-to-end vector for a single arm. The autocorrelation function is fitted to an exponential form, $C_R(t) = C_0 \exp(-t/\tau)$ over the time domain when $C_R(t)$ decays from 1.0 to about 0.1; C_0 and τ are both adjustable fitting parameters (C_0 typically is around 0.9−1.0). Figure 2 presents the obtained τ plotted against $\langle R_g \rangle$ for the star in a log−log plot. The inset in Figure 2 shows an example of determined autocorrelation function. Stars with different number of arms and lengths again collapsed into a single master curve with a dependence of $\tau \sim R_g^{3.0}$. This dependence is expected when star polymers appear as nondraining to the solvent (i.e., the Zimm model as opposed to the Rouse model). From these, one can infer that hydrodynamic interactions are fully developed within the stars in DPD simulations. Additionally, by making use of the R_g dependence on f discussion in the previous paragraph, we would predict that $\tau \sim N_a^{3\nu} f^{3\nu-3}(3f-2)^{3/2}$; at high f, $\tau \sim N_a^{3\nu} f^{3(\nu-1/2)}$. Taking $\nu = 0.59$ for our polymer model, we would predict $\tau \sim N_a^{3\nu} f^{0.27}$ for $f \gg 1$. Therefore, an increase in f would increase the relaxation time of each individual arm. This trend can be seen from data shown in Figure 2. However, we are unable to determine the exact scaling dependence on f due to limited range of f investigated. Several earlier studies investigated dynamics of stars with different simulation methods.[4,8,45] Rey et al. simulated star polymers with Gaussian chain statistics using Brownian dynamics with fluctuating hydrodynamic interaction. Their data could be replotted in the same form, τ vs R_g, and yields an exponent $\tau \sim R_g^{3.4\pm0.1}$, but their data covered a very small range of τ; therefore, the reliability of the exponent is limited. In addition, their raw data showed almost no dependence on the number of arm f. This is consistent with our predicted dependence on f since in their model chains follow Gaussian statistics and hence $\nu = 0.5$, which will lead τ to be independent of f. On the other hand, Grest also reported relaxation times independent of arm number f, which however was not consistent with our results. In Grest's paper, stars have excluded volume interaction but no hydrodynamic interaction between polymer beads. Our polymer chain model has the excluded volume interaction, as evident from the exponent in $R_g^2 \sim N_{tot}^{1.18}$ dependence. Our model, however, also has hydrodynamic interaction. As a result, we observed an increase in τ as the arm number f increases. The dependence of τ on arm length, N_a, simply reflects the usual Zimm model's prediction, $\tau \sim R_g^3$.

3.2. Retention Time in Hydrodynamic Chromatography. The concept of hydrodynamic chromatography (HDC) was

Table 1. Average Velocities of Polymer V_p and Solvent V_s and Relative Retention Time t_r for Stars in a Pipe[a]

	linear ($f = 2$)			$f = 3$			$f = 4$			$f = 5$			$f = 8$		
f_x	$\langle V_p \rangle$	$\langle V_s \rangle$	t_r	$\langle V_p \rangle$	$\langle V_s \rangle$	t_r	$\langle V_p \rangle$	$\langle V_s \rangle$	t_r	$\langle V_p \rangle$	$\langle V_s \rangle$	t_r	$\langle V_p \rangle$	$\langle V_s \rangle$	t_r
0.005	0.311	0.2526	0.812	0.317	0.2520	0.794	0.317	0.2518	0.794	0.3304	0.2512	0.7605	0.3368	0.2495	0.7407
0.008	0.480	0.4046	0.843	0.511	0.4037	0.790	0.522	0.4026	0.770	0.5346	0.4016	0.7513	0.5546	0.4002	0.7215
0.01	0.610	0.5056	0.829	0.648	0.5044	0.779	0.653	0.5033	0.770	0.6618	0.5025	0.7593	0.7048	0.4999	0.7092
0.03	1.886	1.513	0.8025	2.007	1.511	0.7524	2.091	1.509	0.7215	2.188	1.507	0.6887	2.284	1.502	0.6579
0.05	3.305	2.514	0.7605	3.516	2.510	0.7143	3.707	2.508	0.6766	3.813	2.505	0.6570	3.969	2.499	0.6297

[a] All data are obtained for stars with $N_a = 10$ in a pipe with radius $R_p = 10.0r_c$. All errors are on the last digit of the numbers.

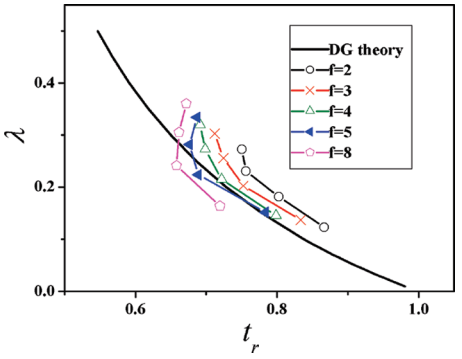

Figure 3. Computational determined relative retention time $t_r = \langle V_p \rangle / \langle V_s \rangle$ against $\lambda = R_{g0}/R_p$ for stars with different number of arms f and arm length $N_a = 5, 10, 15$ and 20, $f_x = 0.03k_BT/r_c$, $R_p = 10.0r_c$, and $\lambda = R_{g0}/R_p$ where R_{g0} is the radius of gyration of stars determined in dilute bulk solution and R_p is the radius of the pipe. The solid line is the prediction according to Dimarzi−Guttman's theory.

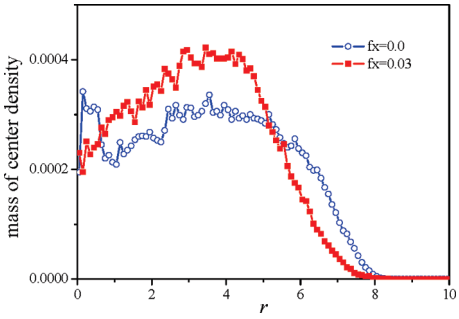

Figure 4. Center-of-mass density distribution of star polymers at $f_x = 0.0k_BT/r_c$ (blue circle) and $f_x = 0.03k_BT/r_c$ (red square) in a pipe of radius $R_p = 10.0r_c$, number of arms $f = 4$, and arm length $N_a = 15$.

first proposed by Dimarzio and Guttman (DG theory),[46] and it refers to separation of colloidal/macromolecules according to the size achieved by transporting the solution through a channel under pressure-driven flow. The relative retention time t_r of solute is determined according to $t_r = \langle V_s \rangle / \langle V_p \rangle$, where $\langle V_s \rangle$ and $\langle V_p \rangle$ are the average solvent (or marker) and polymer velocities, respectively. We are interested in comparing the relative retention behavior of linear chain and star polymer with nearly the same R_g value. Table 1 compares the average velocity of star polymers with same arm length but different arm numbers at otherwise the same given conditions. The difference in velocities is small, but one can notice that as the number of arms increases, $\langle V_p \rangle$ increases and $\langle V_s \rangle$ decreases slightly. As a result, the retention time t_r decreases with the increase in the number of arms. A better way to view how star architecture affect the retention behavior is by plotting, in a way familiar to experimentalists working with polymer separation, $\lambda = R_{g0}/R_p$ against retention time, t_r, as presented in Figure 3, where R_{g0} is the radius of gyration of the polymer chain estimated in the bulk solution and R_p is the pipe radius. The solid line in the figure is the prediction of retention time according to DG theory, $(t_r)^{-1} = (1 + 2\lambda - C\lambda^2)$, where $C = 1.0$, a number suggested by DG theory when polymer is viewed as impenetrable to solvent. This theory itself does not differentiate linear polymers from star polymers. Hence, we will not compare our simulation results with theoretical predictions here.

From Figure 3, one may observe that the more number of arms in the star, the smaller the retention time, which implies that stars with more arms are eluted earlier. There are two reasons causing the decrease in retention time as number of arms f increase. First, $\langle V_s \rangle$ decreases slightly as f increases, since stars with more arms exert stronger drag on fluid velocity. As a result, the average fluid velocity at the same pressure drop decreases, reflecting an increased viscosity of branched polymer solutions. This factor is small, and it should become even smaller when the volume fraction of the polymer solution is kept very low. The second factor is due to the increased $\langle V_p \rangle$ as f increase. This increase in $\langle V_p \rangle$ can be traced to how star polymers are distributed in the pipe, which will be discussed in the next section.

3.3. Center-of-Mass Density and Velocity Profiles. The distribution of polymers in the channel during flow has been a subject of several recent studies.[32,34,47−54] Discussion has been centered on the migration patterns of polymers during the flow. It has been argued that properly accounting for polymer/wall hydrodynamic interactions should lead to a migration of polymers away from the wall in the presence of flow. Failing to account for this wall hydrodynamic interaction would lead to a migration toward the wall.[49,52−55] In the case of very narrow channel, however, migration toward the wall may occur.[49] Earlier numerical simulations of pressure-driven flow of linear polymer solutions by DPD[32,50] have led to some controversies about the capability to properly account for hydrodynamic interaction with the wall. The generalized DPD model[34] has thus been proposed that seems to predict the migration pattern more consistent with other numerical simulations such as lattice−Boltzmann or Brownian dynamic simulations with hydrodynamic interaction. Specifically, Millan ad Laradji[34] showed that the standard DPD failed to show migration toward the channel center especially when chain length was long. However, by using a generalized DPD that has a Schmidt number around 12, they observed a clear migration toward the channel center under flow, in agreement with numerical results reported by other simulation methods. In the current study, we have used the standard DPD model and the revealed migration pattern may suffer from the low Schmidt effect. Figure 4 compares the center-of-mass density profiles of 4-arm star polymers under quiescent conditions and under flow with $f_x = 0.03k_BT/r_c$. There is a significant migration away from the wall along with a development of off-center peak during the flow. The development of the off-center peak is attributed to the gradient in the shear rate across the channel, which leads to a gradient in chain diffusivity. The migration away from the pipe wall is attributed to hydrodynamic interaction with the wall. This observed migration pattern in Figure 4 is what

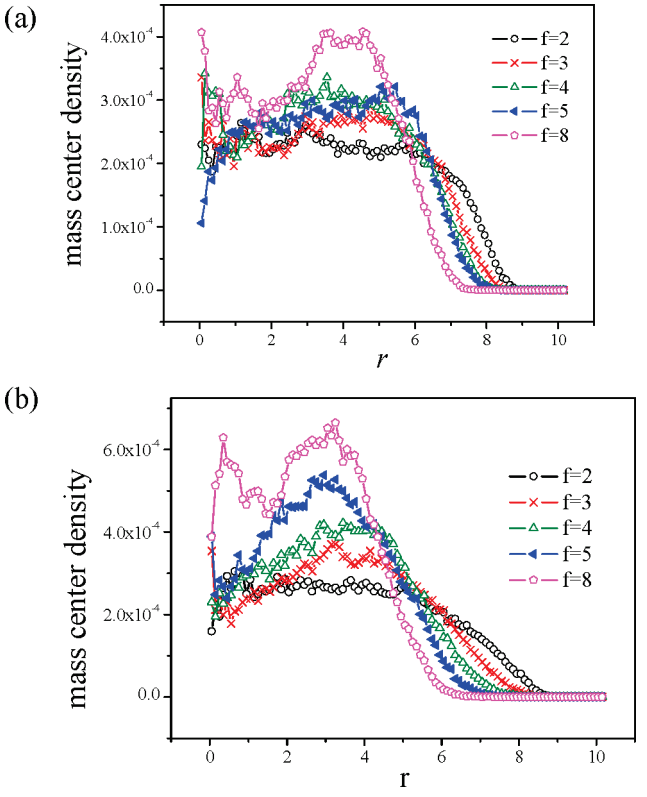

Figure 5. Center-of-mass density distribution of star polymers (N_a = 15) with f varied form 2 to 8. (a) f_x = 0.0; (b) f_x = 0.03 in a pipe of radius R_p = 10.0r_c. The radius of gyration of star polymers in bulk solution R_{g0} = 2.31, 2.56, 2.73, 2.82, and 3.05 respectively for f = 2, 3, 4, 5, and 8.

to be expected if wall/polymer hydrodynamic interaction has been accounted for. We noticed that the corresponding migration pattern for the linear chains (f = 2, data shown in Figure 5), however, did not clearly produce this migration away from the wall, reflecting some inadequacy of standard DPD to simulate transport of polymers. As the arm number increases, the observed migration away from the wall is more pronounced and enhanced. We attribute this to a stronger hydrodynamic interaction between star polymers with the wall. As a result, standard DPD is able to capture this hydrodynamic interaction and produce the correct migration pattern. However, a further study with generalized DPD to examine the migration pattern of star polymers relative to linear polymers probably is needed.

Figure 5 presents the center-of-mass distribution of star polymer with varying number of arms f under quiescent conditions (f_x = 0.0) and under flow (f_x = 0.03). At quiescent conditions (f_x = 0.0; Figure 5a), the depletion layer near the wall gets thicker when f increases. The increase in the depletion layer is more than the amount accounted by simple exclusion due to an increase in R_{g0}, which can be verified by plotting density profiles against reduced radius such as r/R_{g0}. This increased depletion layer at quiescent conditions can be traced to the way how the wall boundary is constructed. In our model, the fluid particles including polymer particles interact with frozen wall particles through regular DPD forces. These forces are long-range interaction, and hence the polymer/wall interaction is long-ranged in nature. Depletion layer formed near the wall is therefore not simply due to entropic exclusion. This effect could already give rise a faster transport and hence shorter retention time of stars relative to linear chains.

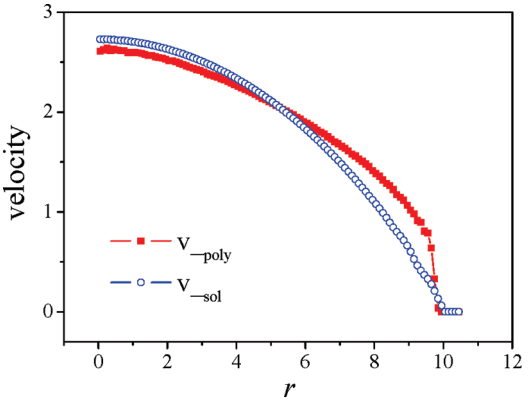

Figure 6. Comparison of velocity profiles for polymer segments and solvent particles in the pipe R_p = 10.0r_c under pressure-driven flow, f_x = 0.03k_BT/r_c. Polymers are 4-arm branched stars with N_a = 15.

Comparing parts a and b of Figure 5 reveals that when the flow is added, the density profiles shifted toward the channel center and the amount of shift is more significant as f increases. Within DPD model, stars with nearly the same size as the linear chains will have more beads and hence stars will have stronger hydrodynamic interaction with the wall. As a result of this stronger hydrodynamic interaction, the migration toward the channel center becomes more pronounced, giving rise to an even faster transport of stars in the pipe. On the other hand, the polymer velocity profiles remain very similar as f increases. We saw very small decrease in polymer velocity profile in the center of pipe and very small increase near the wall as f increases. The extent of change in velocity profiles as f increases is small. The typical velocity profiles for the solvents and polymers at f_x = 0.03k_BT/r_c are presented in Figure 6. Polymer velocity in the center of pipe is slightly retarded than the solvent, whereas near the wall it is slightly enhanced. The extent of difference between these two profiles increase with increased driving force. These data combined together indicate that the faster transport of star polymers observed in DPD simulations is mostly due to enhanced migration of star polymers toward the pipe center as the number of arms increases. This conclusion however is drawn based on results obtained from standard DPD simulation algorithm. In view of issues like Schmidt number on the observed migration pattern, a further study using other simulation methods or modified DPD methods with higher Schmidt number is needed.

3.4. Chain Stretching. Chain stretching during shear flow is another subject that has been under intensive investigation both experimentally and computationally.[56−61] Here we monitored the extent of chain stretching (and compression) during flow by defining three ratios $S_x = 3\langle R_{gx}^2\rangle/\langle R_{g0}^2\rangle$, $S_y = 3\langle R_{gy}^2\rangle/\langle R_{g0}^2\rangle$, and $S_z = 3\langle R_{gz}^2\rangle/\langle R_{g0}^2\rangle$ where R_{gx}^2, R_{gy}^2, and R_{gz}^2 are the mean-square radius gyration of the chains during the flow along the x, y, and z components, respectively, and R_{g0}^2 is the mean-square radius of gyration of chains in dilute bulk solution at quiescent conditions. The conformational statistics of the chain under shear flow depends strongly on the Weissenberg number $Wi = \dot{\gamma}\tau$, where $\dot{\gamma}$ is the shear rate, calculated in the generated Poiseuille flow according to $\dot{\gamma} = 2.0\langle u\rangle/R_p$, $\langle u\rangle$ is the average fluid velocity, and τ is the characteristic relaxation time defined as end-to-center vector relaxation time of the chain in the bulk solution, which is determined in section 3.1.

Figure 7 presents plots of stretch ratio versus the Weissenberg number for linear polymer chains. The chain is stretched along the flow direction (x component) but compressed in

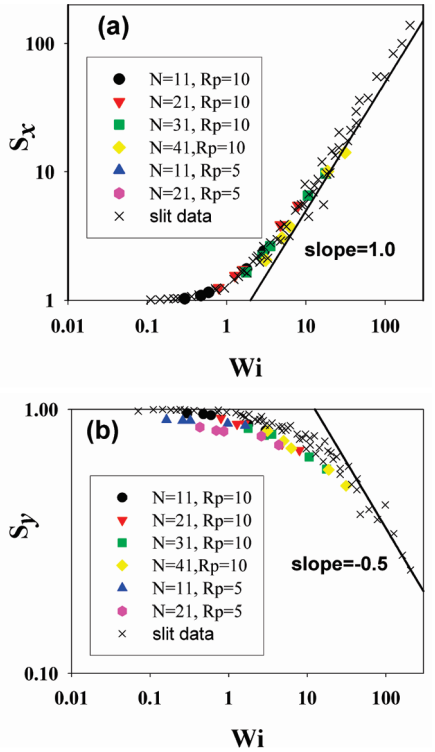

Figure 7. Plots of chain stretch ratio, $S_x = 3\langle R_{gx}^2\rangle/\langle R_{g0}^2\rangle$, and compression factor, $S_y = 3\langle R_{gy}^2\rangle/\langle R_{g0}^2\rangle$, vs Weissenberg number, Wi, for linear polymer chains. Colored data sets are obtained in pipe channel with radius R_p indicated in the legend. Black cross symbols are data sets obtained from transport in a slit channel.

the y and z directions. The plots also contain the data obtained earlier for transport of linear chains in a slit channel[43] formed by two parallel walls separated in the z direction. Whether in a pipe channel or slit channel, the stretching in x direction is independent of channel type and is determined primarily by the Weissenberg number with a power-law dependence $S_x \sim Wi^{1.0}$ when $Wi \gg 1$. In other studies, a slightly different quantity has been used to quantity the stretching of the chain during flow. Ripoll et al.[37] and Hernandez Cifre et al.[62] monitored how $\delta^2 = \langle R_{gx}^2\rangle/\langle R_{gx}(0)^2\rangle - 1$, which is equivalent to our $S_x - 1$, changes with the shear rate. Ripoll et al. showed a 2.0 power-law dependence at low Weissenberg number (less than 10.0), but crossover to 1.0 power-law dependence at high Weissenberg number. This is in agreement with what we have observed here since from Figure 7 one can clearly see that there is a crossover region from nonstretched state to highly stretched scaling region of 1.0 power law. The compressions in the y and z components are influenced by the channel type. In a slit channel, compression in the z component where the walls are present is stronger than the compression in the y component. In the pipe channel, the y and z components are compressed to the same extent. One may observe that data for the pipe in Figure 7b do not overlap well with that in the slit channel, but the two are very close. The exponent in the power-law dependence for S_y on Wi at large Wi is less certain because of limited range of data available, and we estimated to be around -0.5 using data at high Wi number. In addition, the scaling plots presented in Figure 7 are not perfect. Data sets obtained in pipes with different radii do not overlap perfectly, especially when R_p becomes comparable with sizes of polymers. In fact, we have limited data sets to those when $R_p/R_{g0} > 2$ in Figure 7. The imperfection in the scaling plot may be attributed to nonuniform shear in Poiseuille flow. Also,

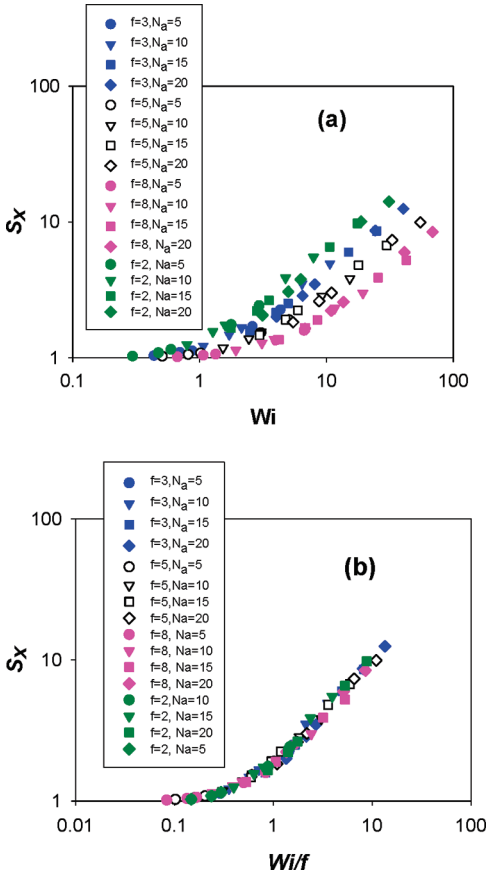

Figure 8. (a) Plot of stretch ratio S_x versus Weissenberg number for stars with arms $f = 2$, 3, 5, and 8. (b) Same data as in (a) but plotted against Weissenberg number reduced by arm number f. All data are obtained in a pipe of radius $10r_c$, which is greater than polymer size.

the stretching of chain may have distinctly different behavior when pipe radius becomes comparable to or smaller than the polymer size, as investigated recently by Cannavacciuolo et al.[63]

Data in Figure 7 could be compared with experimental results by Teixeira et al.,[58] who monitored the stretching and compression of DNA chains under simple shear flow experimentally. Their compression factor, defined as $\langle\delta_2\rangle/\langle\delta_{2,0}\rangle$, is equivalent to our $(S_y)^{1/2}$. They reported that the compression factor depends on Weissenberg number with a power of -0.26, which compares well with our data. For the stretching in the flow direction, these authors also obtained a master plot for the fractional of extension, $\langle x\rangle/L$, as a function of Weissenberg number, but they did not discuss the power-law dependence. Ripoll et al.,[37] however, reported a linear dependence of $S_x \sim Wi^{1.0}$ when $Wi > 1$ for star polymers, but the same power-law dependence is likely to be true for the linear polymers (as will be shown later). Most of earlier studies of chain stretching in shear flow has focused on fractional extension $\langle x\rangle/L$ since one might expect the chain stretch will be limited by the contour length of the chain. In elongational flow, fractional extension reaches a plateau value as high as 0.9 when $Wi > 1$, but in shear flow, the fractional extension never exceeds 0.5 in experiments. If the power-law dependence is valid at high Wi, it is not clear to us how the chain stretch may be limited by the contour length. Currently, we are not certain of the theoretical justification of this power law dependence.

Figure 8a compares the stretching of star polymers with linear polymers, monitored in the same way as in Figure 7a.

Stars with the same arm number f but different arm length form a single curve, but each curve is shifted toward right as f increases. We note the Weissenberg number Wi used in Figure 8a adsorbs some effect of stars architecture since τ used here is the relaxation time of the center-to-end vector for the stars, which increases as f increases. However with Wi thus defined, the stretch of stars is delayed as f increases. These curves however can be collapsed when the Wi number is reduced by f, as shown in Figure 8b. As far as we know, this is the first report of such dynamic rescaling for stars polymers. Ripoll et al. have shown that stretching S_x is delayed as f increases, but they did not show whether such rescaling would work for stretching ratio S_x. They however have shown that rotational frequency of the star polymers in shear flow, which depends on Wi as well, can be collapsed together by using a rescaled Weissenberg number, $\phi(f)Wi$, where the parameter $\phi(f)$ varied from 2 to 1 for arm numbers f varied from 5 to 50. Our simulation data presented in Figure 7b contain only data sets with f varied from 2 to 8, a relatively small range. Whether the same reduced Weissenberg number would work at high f is unknown and will be examined in the future simulations. The compression factor S_y follows the same scaling plots when plotted against Wi/f (data not shown).

In the case of linear polymers, the chain dimension along the flow direction fluctuates significantly. The chain shrinks and tumbles in the shear flow. For star polymers, the overall chain dimension along the flow direction fluctuates less although individual arm undergoes similar shrink and extension. As suggested by Ripoll et al., the stars undergo tanklike threading motion in the flow. Analysis of the rotational frequency of stars will be presented in the future.

4. Conclusions

We have examined the transport of star polymers in a pipe with radius at least twice the size of star polymers using standard dissipative particle dynamics simulations. We are interested in the transport of star polymers from two perspectives. First we want to compare the relative retention time of stars with respect to linear polymers during the pressure-driven flow (i.e., the so-called on-chip hydrodynamic chromatography separation). Our simulations reveal that stars travel faster than the linear polymers with approximately the same size, leading to retention time of stars being smaller than that of linear chains in HDC. The smaller retention time is traced to the fact that stars are migrated further away from the walls during the flow. Hence, stars sample a narrower region of velocity profile in the center of pipe with faster velocity, which leads to a net higher average velocity of the stars. In our current study, we have used the standard DPD which has a Schmidt number on the order of one. Although the absolute migration patterns of linear polymer chains were shown to depend on the Schmidt number, we note that we focus on the comparison of relative migration pattern of stars against the linear chains. The trend we observed here is likely to hold even if we use modified DPD with a higher Schmidt number; however, a further study with modified DPD probably is needed to clarify this point.

We further investigated the stretching behavior of the chains during the pressure-driven flow by examining stretching factor, $S_x = \langle R_{gx}{}^2\rangle/\langle R_{gx0}{}^2\rangle$, and compression factor perpendicular to the flow, $S_y = \langle R_{gy}{}^2\rangle/\langle R_{gy0}{}^2\rangle$. Both S_x and S_y depend on Weissenberg number Wi, $S_x \sim Wi^{1.0}$, whereas $S_y \sim Wi^{-0.5}$ when $Wi \gg 1$. For the star polymers, the stretch is delayed as the number of arms f increases. However, by using a modified Weissenberg number, Wi/f, the stretching and compression behavior of stars can be collapsed with the data for the linear chains. The reported data cover only stars with number of arms no greater than 10. Whether the same type of dynamic rescaling would apply for stars with high number of arms needs to be further investigated.

Acknowledgment. In the US, this work was partially supported by funding from ACS/PRF (PRF# 46933-AC7) and from National Science Foundation under Grant CHE-0724117 (cofunded by MPS/CHE and OISE). In China, this work was supported by the National Natural Science Foundation of China (20734003) Programs and the Fund for Creative Research Groups (50921062). Ziqi Li was an exchange graduate student between China and US investigators.

References and Notes

(1) Zimm, B. H.; Stockmayer, W. H. *J. Chem. Phys.* **1949**, *17*, 1301–14.
(2) Daoud, M.; Cotton, J. P. *J. Phys.* (*Paris*) **1982**, *43*, 531–8.
(3) Birshtein, T. M.; Zhulina, E. B. *Polymer* **1984**, *25*, 1453–61.
(4) Grest, G. S.; Kremer, K.; Witten, T. A. *Macromolecules* **1987**, *20*, 1376–83.
(5) Halperin, A.; Alexander, S. *Macromolecules* **1987**, *20*, 1146–1152.
(6) Batoulis, J.; Kremer, K. *Macromolecules* **1989**, *22*, 4277–4285.
(7) Freire, J. J.; Rey, A.; Bishop, M.; Clarke, H. R. *Macromolecules* **1991**, *24*, 6494–6499.
(8) Grest, G. S. *Macromolecules* **1994**, *27*, 3493–500.
(9) Shida, K.; Ohno, K.; Kimura, M.; Kawazoe, Y.; Nakamura, Y. *Macromolecules* **1998**, *31*, 2343–2348.
(10) Molina, L. A.; Freire, J. J. *Macromolecules* **1999**, *32*, 499–505.
(11) Zifferer, G. *Macromol. Theory Simul.* **1999**, *8*, 433–462.
(12) Sikorski, A. *Macromolecules* **2002**, *35*, 7132–7137.
(13) Teraoka, I. *Polymer Solutions: An Introduction to Physical Properties*, 1st ed.; Wiley-Interscience: New York, 2002.
(14) Rubinstein, M.; Colby, R. H. *Polymer Physics*; Oxford University Press: New York, 2003.
(15) Zimm, B. H. *Macromolecules* **1980**, *13*, 592–602.
(16) Zimm, B. H. *Macromolecules* **1984**, *17*, 795–798.
(17) Wilkinson, M. K.; Gaunt, D. S.; Lipson, J. E.; Whittington, S. G. *Macromolecules* **1988**, *21*, 1818–1822.
(18) Freire, J. J.; Molina, L. A.; Rey, A.; Adachi, K. *Macromol. Theory Simul.* **1999**, *8*, 321–327.
(19) Xu, G.; Mattice, W. L. *Macromol. Theory Simul.* **2002**, *11*, 649–654.
(20) Dunweg, B. *J. Chem. Phys.* **1993**, *99*, 6977–6982.
(21) Groot, R. D.; Warren, P. B. *J. Chem. Phys.* **1997**, *107*, 4423–4435.
(22) Espanol, P.; Warren, P. *Europhys. Lett.* **1995**, *30*, 191–196.
(23) Hoogerbrugge, P. J.; Koelman, J. M. V. A. *Europhys. Lett.* **1992**, *19*, 155–160.
(24) Malevanets, A.; Kapral, R. *J. Chem. Phys.* **2000**, *112*, 7260–7269.
(25) Malevanets, A.; Kapral, R. *J. Chem. Phys.* **1999**, *110*, 8605–8613.
(26) Mussawisade, K.; Ripoll, M.; Winkler, R. G.; Gompper, G. *J. Chem. Phys.* **2005**, *123*, 144905.
(27) Benzi, R.; Succi, S.; Vergassola, M. *Phys. Rep.* **1992**, *222*, 145–197.
(28) Ahlrichs, P.; Dunweg, B. *J. Chem. Phys.* **1999**, *111*, 8225–8239.
(29) Ahlrichs, P.; Dunweg, B. *Int. J. Mod. Phys. C* **1998**, *9*, 1429–1438.
(30) Slater, G. W.; Holm, C.; Chubynsky, M. V.; de Haan, H. W.; Dube, A.; Grass, K.; Hickey, O. A.; Kingsburry, C.; Sean, D.; Shendruk, T. N.; Zhan, L. *Electrophoresis* **2009**, *30*, 792–818.
(31) Lowe, C. P. *Europhys. Lett.* **1999**, *47*, 145–151.
(32) Fan, X.; Phan-Thien, N.; Chen, S.; Wu, X.; Ng, T. Y. *Phys. Fluids* **2006**, *18*, 063102.
(33) Symeonidis, V.; Karniadakis, G. E.; Caswell, B. *J. Chem. Phys.* **2006**, *125*, 184902.
(34) Millan, J. A.; Laradji, M. *Macromolecules* **2009**, *42*, 803–810.
(35) Jiang, W.; Huang, J.; Wang, Y.; Laradji, M. *J. Chem. Phys.* **2007**, *126*, 044901/1–044901/12.
(36) Ripoll, M.; Winkler, R. G.; Gompper, G. *Eur. Phys. J. E* **2007**, *23*, 349–354.
(37) Ripoll, M.; Winkler, R. G.; Gompper, G. *Phys. Rev. Lett.* **2006**, *96*, 188302−1–188302−4.
(38) Nardai, M. M.; Zifferer, G. *J. Chem. Phys.* **2009**, *131*, 124903.
(39) Chmela, E.; Tijssen, R.; Blom, M. T.; Gardeniers, H. J. G. E.; van den Berg, A. *Anal. Chem.* **2002**, *74*, 3470–3475.
(40) Chmela, E.; Blom, M. T.; Gardeniers, J. G. E.; van den Berg, A.; Tijssen, R. *Lab Chip* **2002**, *2*, 235–241.
(41) Blom, M. T.; Chmela, E.; Oosterbroek, R. E.; Tijssen, R.; van den Berg, A. *Anal. Chem.* **2003**, *75*, 6761–6768.

(42) Stein, D.; van der Heyden, F. H.; Koopmans, W. J.; Dekker, C. *Proc. Natl. Acad. Sci. U.S.A.* **2006**, *103*, 15853–8.
(43) Wang, Y.; Jiang, W.; Miller, S.; Eckstein, E. *J. Chromatogr., A* **2008**, *1198*, 140–147.
(44) Huang, J.; Wang, Y.; Laradji, M. *Macromolecules* **2006**, *39*, 5546–5554.
(45) Rey, A.; Freire, J. J.; Garcia de la Torre, J. *Macromolecules* **1990**, *23*, 3948–53.
(46) Dimarzio, E. A.; Guttman, C. M. *J. Chromatogr.* **1971**, *55*, 83–97.
(47) Usta, B. O.; Ladd, A. J. C.; Butler, J. E. *J. Chem. Phys.* **2005**, *122*, 094902−1–094902−11.
(48) Khare, R.; Graham, M. D.; De Pablo, J. J. *Phys. Rev. Lett.* **2006**, *96*, 224505/1–224505/4.
(49) Usta, B. O.; Buter, J. E.; Ladd, A. J. C. *Phys. Fluids* **2006**, *18*, 031703−1/–31703−4.
(50) Millan, J. A.; Jiang, W.; Laradji, M.; Wang, Y. *J. Chem. Phys.* **2007**, *126*, 124905/1–124905/9.
(51) Ladd, A. J. C.; Kekre, R.; Butler, J. E. *Phys. Rev. E* **2009**, *80*, 036704.
(52) Chen, Y. L.; Ma, H.; Graham, M. D.; de Pablo, J. J. *Macromolecules* **2007**, *40*, 5978–5984.
(53) Chen, Y. L.; Graham, M. D.; De Pablo, J. J.; Jo, K.; Schwartz, D. C. *Macromolecules* **2005**, *38*, 6680–6687.
(54) Jendrejack, R. M.; Schwartz, D. C.; de Pablo, J. J.; Graham, M. D. *J. Chem. Phys.* **2004**, *120*, 2513–2529.
(55) Ma, H.; Graham, M. D. *Phys. Fluids* **2005**, *17*, 083103/1–083103/13.
(56) Perkins, T. T.; Smith, D. E.; Chu, S. *Science* **1997**, *276*, 2016–21.
(57) Smith, D. E.; Babcock, H. P.; Chu, S. *Science* **1999**, *283*, 1724–1727.
(58) Teixeira, R. E.; Babcock, H. P.; Shaqfeh, E. S. G.; Chu, S. *Macromolecules* **2005**, *38*, 581–592.
(59) Schroeder, C. M.; Babcock, H. P.; Shaqfeh, E. S. G.; Chu, S. *Science* **2003**, *301*, 1515–1519.
(60) Schroeder, C. M.; Shaqfeh, E. S. G.; Chu, S. *Macromolecules* **2004**, *37*, 9242–9256.
(61) Schroeder, C. M.; Teixeira, R. E.; Shaqfeh, E. S. G.; Chu, S. *Macromolecules* **2005**, *38*, 1967–1978.
(62) Hernandez Cifre, J. G.; Pamies, R.; Lopez Martinez, M. C.; Garcia de la Torre, J. *Polymer* **2005**, *46*, 6756–6766.
(63) Cannavacciuolo, L.; Winkler, R. G.; Gompper, G. *Europhys. Lett.* **2008**, *83*, 34007/1–34007/6.